Syntheses, crystal structures, photo-physical properties, antioxidant and antifungal activities of Mg(II) 4,4'-bipyridine and Mg(II) pyrazine complexes of the 5,10,15,20 tetrakis(4–bromophenyl)porphyrin

N. Amiri, F. Ben Taheur, S. Chevreux, C.M. Rodrigues, V. Dorcet, Gilles Lemercier, H. Nasri

Syntheses, crystal structures, photo-physical properties, antioxidant and antifungal activities of Mg(II) 4,4'-bipyridine and Mg(II) pyrazine complexes of the 5,10,15,20 tetrakis(4-bromophenyl)porphyrin.

Nesrine Amiri [a*], Fadia Ben Taheur [b], Sylviane Chevreux [c,d], Carine Machado Rodrigues [c], Vincent Dorcet [e], Gilles Lemercier [c], and Habib Nasri [a]

[a] *Laboratory of Physical Chemistry of Materials, University of Monastir, Avenue of the Environment, 5019 Monastir, Tunisia.*

[b] *Laboratory of Analysis, Treatment and Valorisation of Environmental Pollutants and Products, Faculty of Pharmacy, Monastir University, Tunisia.*

[c] *University of Reims Champagne Ardenne, ICMR UMR CNRS 7312, BP 1039-51687, Reims Cedex 2, France.*

[d] *Chimie Paris Tech, PSL University, CNRS, Institut de Recherche de Chimie Paris, 75005 Paris, France*

[e] *Institute of Chemical Sciences of Rennes, UMR 6226, University of Rennes 1, Beaulieu Campus, 35042 Rennes, France.*

Received date (to be automatically inserted after your manuscript is submitted)
Accepted date (to be automatically inserted after your manuscript is accepted)

ABSTRACT: This study concerns the synthesis of 5,10,15,20-tetrakis(4-bromophenyl)porphyrin (H_2TBrPP)-based magnesium(II) complexes involving 4,4'-bipyridine (4,4'-bpy) and pyrazine (pyz) ligand, for [Mg(TBrPP)(4,4'-bpy)] (**1**) and [Mg(TBrPP)(pyz)$_2$] (**2**), respectively. New complexes **1** and **2** were characterized by single crystal X-ray diffraction, elemental analysis, infrared and nuclear magnetic resonance spectroscopies. The photo-physical properties were investigated by UV-visible absorption and emission spectroscopies. These new magnesium(II) complexes exhibit promising antifungal and antioxidant activities.

KEYWORDS: porphyrin-based Mg(II) complexes; pyrazine ligand; 4,4'-bipyridine ligand; X-Ray structures; photo-physical properties; antioxidant and antifungal activities.

*Correspondence to: Nesrine Amiri, telephone +(216) 28 25 64 32, fax: +(216) 73 50 02 78, nesamiri@gmail.com

I NTRODUCTION

Porphyrins and their metal complexes were considered as active materials used in polymerization [1-3] and they also exhibited important function as catalysts, in medicinal and pharmaceutical fields [4-6], and functional dyes and pigments [7]. For example, iron and manganese porphyrinic complexes were used as efficient catalysts for hydroxylation of alkanes and epoxidation of alkenes [8-14]. Having conjugated configuration, porphyrins and metalloporphyrins are remarkable precursors in supramolecular chemistry [15,16] and are considered as excellent components in the design of functional molecular materials with improved electrochemical and physical-chemical properties [16]. Several projects were reported, including molecular wires [17], chemical sensors [18], semi-conductors [19], photo-induced electron transfer [20,21], and solar photovoltaic cells [22,23]. Notably several derivatives based on porphyrin had been developed as efficient photosensitizers for photodynamic therapy (PDT) in clinical applications [24,25]. Structures of magnesium porphyrins are also of interest because of their relationship to chlorophyll, as highlighted in a recent report [26]. Nature selects metal magnesium for chlorophyll type light harvesting molecules, so that non-redox magnesium helps in the light harnessing process. The magnesium complexes attract much attention mainly due to promising photo-physical properties [27,28], and these properties underlie the interest of the latter as potential photosensitizers [29]. Interestingly, Mg(II) porphyrin can easily bind with N/O-donor ligands to produce both five- and six-coordinate complexes [30-34]. Recently, we also reported the preparation of one magnesium derivatives [Mg(TBrPP)(HIm)] five-coordinate [35] and two six-coordinate magnesium complexes [Mg(TPBP)$(L)_2$] (TPBP = 5,10,15,20-tetrakis[4(benzoyloxy)phenyl]porphyrin and L = Hexamethylenetetramine -HTMA- or 1,4-diazabicyclo[2.2.2]octane –DABCO-) [36]. In this context, it was pointed out that these complexes possess interesting activities against several bacterial species including *Escherichia coli*, *Staphylococcus aureus*, *Bacillus subtilis* and *Pseudomonas aeruginosa*. Some examples of magnesium porphyrin-based coordination dimers, oligomers [37] and polymers [38,39] have been designed, many of which based on the axial coordination to the magnesium ion of a metallo-porphyrin through the nitrogen atoms of a bidentate ligand. As development of brominated porphyrin have been
the subject of particular attention due to their catalytic [40,41], electrochemical and optical characteristics [42-45], in this paper and in continuation to our work on functionalization of halogen-substituted porphyrins [35,46], we further combined the porphyrin framework Mg(TBrPP) (TBrPP = 5,10,15,20-tetrakis(4-bromophenyl)porphyrin) with two nitrogen based ligands (4,4'-bpy and pyz) in order to design two novel Mg(II) porphyrins complexes. X-ray diffraction, spectral and photophysical studies were performed for these synthetic compounds. Single crystal X-ray diffraction elucidates the coordination of the Mg(II) ion within these two novel *meso*-porphyrin complexes, bearing 4,4'-bpy and pyz molecules in axial positions to complete the ligand sphere. As far as single crystal structure is concerned, Mg^{2+} ion is penta-coordinated in **1** in the form of [Mg(TBrPP)(4,4'-bpy)], while the same metallic ion is involved in six bonds in **2**, leading to the [Mg(TBrPP)$(pyz)_2$] complex (Fig. 1). These compounds crystallise within the same space group (C2/c). This study provides further information about the structures of these pyramidal and octahedral complexes. UV-visible absorption and emission spectroscopies were also investigated to try to confirm the coordination state of these structures in diluted solution. Proton nuclear magnetic resonance (^{1}H NMR) spectroscopy, tends to show that these complexes seem to be organized in a polymeric (or oligomeric) assembling in these more concentrated $CDCl_3$ solutions.

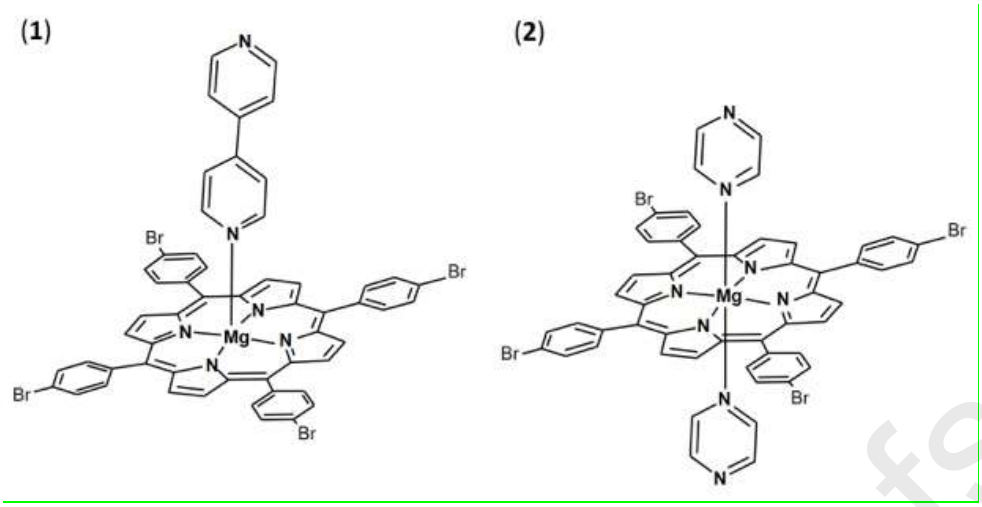

FIGURE 1 Molecular structures of [Mg(TBrPP)(4,4'-bpy)] (**1**) and [Mg(TBrPP)(pyz)$_2$] (**2**).

The synthesized complexes were screened *in vitro* for their antifungal activity to evaluate their inhibiting potential against fungal species including three yeasts strains (*C. krusei*, *C. albicans* and *C. neoformans*) and two fungal strains (*A. brasiliensis* and *A. fumigatus*). The antioxidant activity of the complexes was also investigated through scavenging effect on 1,1-diphenyl-2-picrylhydrazyl (DPPH) radicals.

MATERIALS AND METHODS

Spectroscopies, spectrometry and photo-physical measurements

^{1}H NMR spectra were recorded on a Bruker (Advance 400dpx spectrometer) at 400 MHz. FT-IR spectra were recorded in the region of 400−4000 cm^{-1} on a Nicolet Impact 410 spectrophotometer. UV-Vis spectra were measured with a Varian Cary 5000 spectrophotometer and fluorescence spectra and quantum yield measurements were performed using a Varian Cary Eclipse luminescence spectrophotometer. Elemental analyses were carried out on a Flash EA 1112 Series Thermo Electron fitted with a Porapak column 2m PTFE + MX5 microbalance Mettler Toledo. MALDI-ToF-MS measurements were performed using a SYNAPT G2-Si option MALDI (Waters Corp., Manchester, UK) equipped with a 337 nm UV nitrogen laser producing 3-ns pulses. The samples were also analyzed by ESI/Q-ToF HRMS method, performed on a Waters SYNAPT G2-Si High Resolution Mass Spectrometry equipped with electrospray ionization (ESI) source (Waters Corp., Manchester, UK).

X-ray diffraction study

Crystals of complexes (**1**) and (**2**) suitable for single crystal X-ray diffraction were obtained by methods described above. Purple-blue crystals of dimensions smaller than 0.2 mm were selected for the X-ray diffraction experiment. Data collections for (**1**) and (**2**) were performed on a Bruker APEX-II diffractometer and a Bruker D8 Venture diffractometer, respectively. All diffractometers were equipped with graphite monochromated Mo Kα radiation (λ = 0.71073 Å) and intensity data for all compounds were collected by the narrow frame method at low temperature (150 and 100 K respectively). All structures were solved by direct method using SIR97 and SHELXS-97 [47, 48] and refined by full-matrix least-squares on F_2 using the SHELXL-97 program [48]. Data were corrected for absorption effects by the Multi-Scan method (SADABS) [49]. The crystallographic data are available free of charge on the Cambridge Crystallographic Data Centre (CCDC), under references 1824510 (**1**) and 1877063 (**2**).

Antioxidant activity by 1,1-diphenyl-2-picrylhydrazyl (DPPH) method

The antioxidant activity of the free base porphyrin and their magnesium complexes was evaluated using DPPH radical scavenging activity method. In the experiments, different concentrations (25, 50, 75 and 100 µg/mL) of our compounds were prepared. A volume of 2 mL of each sample was mixed with 2 mL of 0.1 M sodium acetate buffer (pH=5.5). Then, 1 mL of 0.5 M methanol DPPH solution was added. The reaction mixture was shaken vigorously and kept in completely dark for 30 min. Then the absorbance was measured at 517 nm in a spectrophotometer. The percentage of radical scavenging activity (RSA %) was calculated according to the following equation:

$$RSA\ \% = [(AC - AS)/AC]\ x\ 100$$

Where, AC is the absorbance of the control (methanol DPPH solution) and AS is the absorbance of the sample.

Antifungal Activity

Yeasts Strains: three yeasts strains, *C. krusei* ATCC6258, *C. albicans* ATCC90028 and *C. neoformans* ATCC14116 were cultured on Sabouraud agar at 37 °C (optimal temperature for yeast growth) for 48 h. Then, pure colonies were suspended in 10 mL of physiological medium (9 g NaCl in 1 L distilled water), mixed well for 5 min and suspensions were adjusted to 0.5 McFarland standard turbidity. One milliliter of yeast suspension was spread over Sabouraud agar medium plates and incubated for 30 min at 37 °C. Then, 6 mm diameters wells were dug in agar medium using sterile glassy borer. The Mg(II) complexes were prepared in DMSO (1 mg/mL) and introduced into the respective wells, one of the wells was supplemented with DMSO as control. These plates were placed in a 37 °C incubator for 48 h to allow yeast growth. After 48 h, the diameters of the clear zone of inhibition surrounding the sample were measured in millimeters by digital caliper.

Fungal Strains: two fungi strains, *A. brasiliensis* ATCC16404 and *A. fumigatus* ATCC204305 were cultured on inclined Sabouraud agar in Falcon tube 15 mL at 25 °C for 7 days (optimal temperature for their growing). The spore of fungal strain was suspended in peptone water and counted to have 10^6 spores/mL. Then, one milliliter of fungal suspension was spread over Sabouraud agar medium plates and incubated for 30 min at 25 °C. After that, 6 mm diameters wells were dug in agar medium using sterile glassy borer. The Mg(II) complexes were prepared in DMSO (1 mg/mL) and introduced into the respective wells, one of the wells was supplemented with DMSO as control. These plates were placed in a 25 °C incubator for five days to allow fungal growth. After five days, the diameters of the clear zone of inhibition surrounding the sample were measured in millimeters by digital caliper.

Syntheses and crystallization

Commercially available chemicals and reagents were used without purification. The solvents were purified using the available literature methods [50]. The synthesis of 5,10,15,20-tetrakis(4-bromophenyl)porphyrin macrocycle (H_2TBrPP) was performed according to method already described in the literature [51]. The insertion of the magnesium ion into porphyrin molecule was done by the heterogeneous method reported by Lindsey and co-workers [52].

Meso-tetrakis(4-bromophenyl)porphyrin (**H_2TBrPP**): 4-Bromobenzaldehyde (7 g, 37.8 mmol) was dissolved in acetic acid (150 mL) and the solution was heated under reflux conditions. Pyrrole (2.6 mL, 37.8 mmol) was added drop-wise and the dark mixture was heated for a further 30 minutes. After cooling, the black tarry mixture was filtered to obtain a purple solid which, after washing with methanol and water, lead to the porphyrin derivative as purple crystals (15%). ^{1}H NMR [$CDCl_3$, 400 MHz]: δ (ppm) -2.86 (s, 2H, NH_{pyrro}), 7.88 (d, 8H, $^3J_{HoHm}$ = 8.1 Hz, Hm–Hm'), 8.02 (d, 8H, $^3J_{HoHm}$ = 8.1 Hz, Ho–Ho'), 8.80 (s, 8H, Hβ). UV-vis (in CH_2Cl_2) [λ_{max}, nm, (ε, M^{-1} cm^{-1})] 419 (4.52 x 10^6), 515 (2.05 x 10^5), 549 (8.51 x 10^4), 590 (5.88 x 10^4), 648 (4.78 x 10^4). MS [ESI]: m/z calcd for $C_{44}H_{26}Br_4N_4$: 930.32, found: 930.38. FTIR cm^{-1}: 3317 ν(NH porphyrin), 2926 and 2845 ν(CH porphyrin), 966 (δ_{CCH} porphyrin), 731 ν(C–Br porphyrin). Anal. Calcd. for $C_{44}H_{26}Br_4N_4$: C, 56.8; H, 2.81; N, 6.02. Found: C, 56.5; H, 2.79; N, 6.08.

Meso-tetrakis(4-bromophenyl)porphyrinato magnesium(Ii) complex [**Mg(TBrPP)**]: To a solution of free base porphyrin H_2TBrPP (0.5 g, 0.537 mmol) in dichloromethane (80 mL), was added 2 mL of triethylamine followed by 1.35 g (5.25 mmol) of $MgBr_2.OEt_2$. The reaction was stirred at room temperature for 15 minutes. The evolution of this reaction was followed by UV-visible spectroscopy, which highlights the gradual disappearance of a *Q* band. Indeed, the presence of only three *Q* bands is characteristic of a metallated porphyrin [31, 35, 52]. The solvent was evaporated and a light-purple solid of the Mg(TBrPP) complex was obtained (90%). ^{1}H NMR [$CDCl_3$, 400 MHz]: δ(ppm) 7.94 (d, 8H, $^3J_{HoHm}$= 8.35 Hz, Hm–Hm'), 8.09 (d, 8H, $^3J_{HoHm}$= 8.35 Hz, Ho–Ho'), 8.75 (s, 8H, Hβ). UV-vis (in CH_2Cl_2) [λ_{max}, nm, (ε, M^{-1} cm^{-1})] 426 (4.32 x 10^6), 563 (1.69 x 10^5), 603 (1.12 x 10^5), 651 (4.60 x 10^4). Anal. Calcd. for $C_{44}H_{26}Br_4MgN_4$: C, 55.4; H, 2.7; N, 5.9. Found: C, 55.2; H, 2.7; N, 5.6. MS [ESI$^+$]: m/z calcd for $C_{44}H_{25}Br_4N_4Mg$: 951.8552, found: 951.8566. FTIR cm^{-1}: 2969 and 2818 ν(CH porphyrin), 991 ν(δ_{CCH} porphyrin), 720 ν(C-Br porphyrin).

[Mg^{II}(TBrPP)(4,4'-bpy)](4,4'-bpy.H_2O) (**1**): Mg(TBrPP) (20 mg, 0.020 mmol) was mixed with the bidentate ligand 4,4-bipyridine (90 mg, 0.57 mmol) in 5 mL of dichloromethane. The mixture was stirred at room temperature for 3 hours. Crystals were obtained by slow diffusion of *n*-hexane through the dichloromethane solution. ^{1}H NMR [$CDCl_3$, 400 MHz]: δ(ppm) 7.90 (d, 8H, $^3J_{HmHo}$ = 8.4 Hz, Hm–Hm'), 8.01 (d, 8H, $^3J_{HoHm}$ = 8.4 Hz, Ho–Ho'), 8.36 (d, 8H, $^3J_{HbHa}$ = 5.3 Hz, Hb-ligand), 8.54 (d, 8H, $^3J_{HaHb}$ = 5.3 Hz, Ha-ligand), 8.79 (s, 8H, Hβ). UV-vis (in CH_2Cl_2) [λ_{max}, nm, (ε, M^{-1} cm^{-1})]: 427 (4.61 x 10^6), 565 (1.47 x 10^5), 604 (6.60 x 10^4). Anal. Calcd. For $C_{64}H_{42}Br_4MgN_8O$: C, 59.9; H, 3.3; N, 8.7. Found: C, 59.6; H, 3.5; N, 9.0. FTIR cm^{-1}: 3120 ν(CH 4,4'-bpy), 2928 and 2855 ν(CH porphyrin), 1497 ν(CN 4,4'-bpy), 1016 (δ_{CCH} porphyrin), 794 (δ_{CCH} 4,4'-bpy).

[Mg^{II}(TBrPP)(pyz)$_2$]. 0.5 H_2O (2): Mg(TBrPP) (20 mg, 0.020 mmol) and pyrazine (90 mg, 1.1 mmol) in 5 mL of dichloromethane were stirred of 3 hours at room temperature. The colour of the reaction mixture changed from purple to green-blue. Crystals of **2** were prepared by slow diffusion of *n*-hexane into the dichloromethane solution. ^{1}H NMR [$CDCl_3$, 400 MHz]: δ(ppm) 7.14 (s, 8H, Hpyz) 7.96 (d, 8H, $^3J_{HmHo}$ = 8.4 Hz, Hm–Hm'), 8.11 (d, 8H, $^3J_{HoHm}$= 8.4 Hz, Ho–Ho'), 8.81 (s, 8H, Hβ). UV-vis (in CH_2Cl_2) [λ_{max}, nm, (ε, M^{-1} cm^{-1})]: 435 (4.46 x 10^6), 578 (1.69 x 10^5), 618 (1.04 x 10^5). Anal. Calcd. for $C_{52}H_{35}Br_4MgN_8O_{0.5}$ C, 55.6; H, 3.1; N, 10.0. Found: C, 55.6; H, 3.0; N, 9.8. FTIR cm^{-1}: 3061 ν(CH pyz), 2969 and 2918 ν(CH porphyrin), 1482 ν(CN pyz), 998 (δ_{CCH} porphyrin), 794 (δ_{CCH} pyz).

RESULTS AND DISCUSSION

IR and ^{1}H NMR spectroscopies

In order to give more insights in the structure of porphyrin, metalloporphyrin and axially ligated magnesium(II) porphyrin complexes, detailed IR and ^{1}H NMR studies were performed. FTIR spectrum of the free base porphyrin H_2TBrPP (Fig. S7) show a broad band at 3447 cm^{-1}, which is due to overlapping of -NH_2 stretching frequencies, 1472 cm^{-1} due to C=$C_{(aromatic)}$ stretching frequency and the bands observed around 1000 cm^{-1} are assigned to $\delta_{(CCH)}$ vibration modes for the *meso*-porphyrin. This assignment is in good agreement with the work of Boucher and Katz [53]. When the magnesium ion was inserted into the porphyrin ring, the N–H vibration frequency of free base porphyrin disappeared which indicated the formation of magnesium(II) porphyrin compounds (Fig.S6). The IR spectra of the complexes **1** and **2** containing 4,4'-bipyridine and pyrazine as ligands show additional stretching vibration due to the presence of C–H group which lies at 3120 cm^{-1} and 3060 cm^{-1}. Similarly, the bands located in 1485–1480 cm^{-1} spectral range can be attributed to C=N vibrations (Fig. S9 and S10).

^{1}H NMR data of free base porphyrin H_2TBrPP, their corresponding metallated, and axially ligated magnesium(II) porphyrin complexes in $CDCl_3$ at 298 K is listed in Table S1. The free base porphyrin reveals characteristic resonances of β-pyrrole protons as singlet at 8.80 ppm; the NH pyrrole protons are very shielded and are located at -2.86 ppm as low-

intensity singlet, and the aromatic protons of the *meso*-phenyl rings resonate in the 8.02–7.88 ppm region (Fig. S11). The insertion of magnesium metal ion into porphyrin ring shows the absence of inner imino-proton signal and results in the slight shift of resonances towards low field (at higher frequency) (Fig. S12). The ^{1}H NMR spectra of axially ligated [Mg(TBrPP)L] (L= 4,4'-bpy or pyz) are highly characteristic and provide structural information of these compounds in solution. This spectrum shows a slight difference in the proton resonance is observed depending upon the nature of the axial ligand coordinated to the magnesium atom. In the case of [Mg(TBrPP)(4,4'-bpy)] (**1**), Fig. S13 indicates that the *β*-pyrrole protons resonate as a singlet at 8.79 ppm and the *meso*-aryl ortho and meta protons resonate as doublet at 8.01 and 7.90 ppm, respectively, which are slightly deshielded compared to Mg(TBrPP) as well as for H_2TBrPP. The spectrum also reveals other characteristic signals of axial 4,4'-bipyridine ligand. The aromatic protons (C-H) of the 4,4'-bpy ring are shifted to the weak field at 8.54 and 8.36 ppm. Chemical shift and peak integration of Ha and Hb protons of 4,4'-bpy ligand indicates that Mg(TBrPP) complex and 4,4'-bpy ligand form a polymer chain in $CDCl_3$ solution, the repetitive unit being [Mg(TBrPP)(4,4'-bpy)] which have been previously reported in the litterature [38]. Similarly, for compound **2** [Mg(TBrPP)$(pyz)_2$], the *β*-pyrrole protons, the *meso*-aryl ortho and the meta protons resonate at around 8.81, 8.11, and 7.96 ppm, respectively (see Fig. S14). The aromatic protons (C-H) of the pyrazine ring are also shifted to the weak field at around 7.14 ppm. The same behaviour of polymerization in quite concentrated $CDCl_3$ solution (10^{-3} M used for NMR) is highligthed and the repetitive unit being [Mg(TBrPP)(pyz)], observing chemical shift and peak integration of H_{pyz}. To conclude, in solution (concentration in $CDCl_3$ around 10^{-3} M), the NMR characterization is in agreement with a polymeric architecture of both complexes. Due to the high molecular weight of the edifice and the low energy Mg-N_L interaction (axial ligand, see Table 1), mass spectrometry measurements (MALDI-ToF) only allowed us to evidence the parent Mg(TBrPP) motif (see supplementary material in the ESI, Figures. S1-S2 and Figures S3-S4, for compounds **1** and **2**, respectively). This observation is in good agreement with the quite low energy Mg-N_L bond and long Mg-N_L distances; 2.143 Å and 2.350 Å for complex **1** and complex **2**, respectively and compared to an average distance of 2.07 Å for the Mg-N_{porph} bond (see Table 1).

Crystal structure description of compounds 1 and 2

Single crystal XRD analysis of complexes **1** and **2** was done and the data are given in Table S2. Complexes **1** and **2** crystallize in the monoclinic crystal system in the same C2/c space group. Selected bond lengths and angles for both complexes are listed in Table S3. For **1**, the asymmetric unit is made of one half of the [Mg(TBrPP)(4,4'-bpy)] complex, one free 4,4'-bpy molecule and one water molecule. The asymmetric unit of **2** contains half a molecule of the porphyrin, one ligand pyrazine molecule coordinated to the magnesium(II) center and one half free molecule of the same ligand. As shown in Table 1, magnesium metalloporphyrins with monodentate axial ligands are present in solid state as five-coordinate species type [Mg(Porph)(X)] (X = neutral or anionic ligand) in most cases [30,31,35] and as six-coordinate derivative type [Mg(Porph)$(L)_2$] (L = neutral axial monodentate ligand) in few cases *i.e.* [Mg(TPP)$(py)_2$] [54] and [Mg(TPP)$(4\text{-pic})_2$] complexes (TPP = 5,10,15,20-tetraphenylporphyrin, py = pyridine and 4-pic = 4-picoline) [34]. Previously, a linear one-dimensional (1D) polymeric chains of magnesium tetra-porphyrins mediated by bipyridine and pyrazine ligands have been observed in the X-ray structure of the six-coordinate complexes in which Mg-porphyrins units are aligned parallel [38,55]. In the case of tetrakis(ethyl-4(4-butyryl)oxypheny)porphyrine (H_2TEBOP) [56] and (4,4′-bipyridine)(5,10,15,20-tetratolylphenylporphyrinato)zinc(II) [57], Zn(II) complexes with penta-coordination was evidenced. In these reported structures, the zinc(II) is coordinated with 4 N of the porphyrin ring and the N atom of the 4,4′-bipyridine axial ligand, forming a pyramid as a coordination polyhedra of zinc(II). To the best of our knowledge, our study is the first attempt to determine the crystal structure of a five-coordinate Mg(II) complex, (Mg-porphyrin)(4,4'-bpy), (4,4'-bpy = 4,4'-bipyridine) and the crystal structure of a six-coordinate complex, (Mg-porphyrin)(pyz), (pyz = pyrazine). The type of solid state structure formed is directed by the nature of the ligand (especially its electronic

properties) and may be the solvent used. The structure of complex **1** involving a 4,4'-bipyridyl ligand, Mg-porphyrin, which is coordinated by one nitrogen atom (N_{57}) of a pyridine cycle to the magnesium atom forms a five-coordinate complex. On the other hand, the pyrazine ligand which leads to the formation of a six-coordinate complex through coordination of Mg-porphyrin, by one nitrogen atom (N_3) of a first pyrazine heterocycle and the nitrogen atom (N_{3i}) of a second pyrazine. It has to be pointed out that the same trend concerning the difference in coordination mode of 4,4'-bipyridine and pyrazine ligand was already reported in the literature for *meso*-{tetrakis[4-(benzoyloxy)phenyl]porphyrinato} zinc(II) complexes [58].

The ORTEP drawings of **1** and **2** are illustrated by Fig. 2 and 3. First, it has to be pointed out that one molecule of the free ligand (in excess for the synthesis) is present in both structures (Crystals were obtained from the reaction *media*, before purification); it may has a role in the stabilization of the structure *via* H bonds, that are depicted below and in the supplementary material (see Fig. S16 and S18 in the ESI). The coordination geometry around the Mg(II) cation in **1** is pyramid with a square base (Fig. 2), where the four donor N atoms of pyrrole rings of the TBrPP porphyrin occupy the equatorial positions. The donor N atom of axial 4,4'-bpy ligand occupy the apical position.

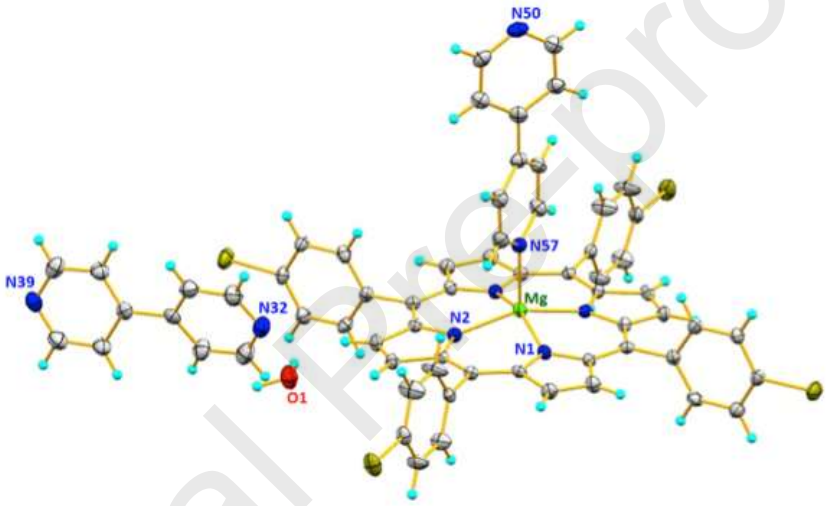

FIGURE 2 ORTEP diagrams of complex **1**. Ellipsoids are drawn at the 40%.

For compound **2**, the close interaction sphere of the Mg(II) cation is described as a distorted octahedron, in which the equatorial positions are occupied by four pyrrole nitrogen atoms and the other two come from two N-donor atoms of the pyrazine ligand (Fig. 3).

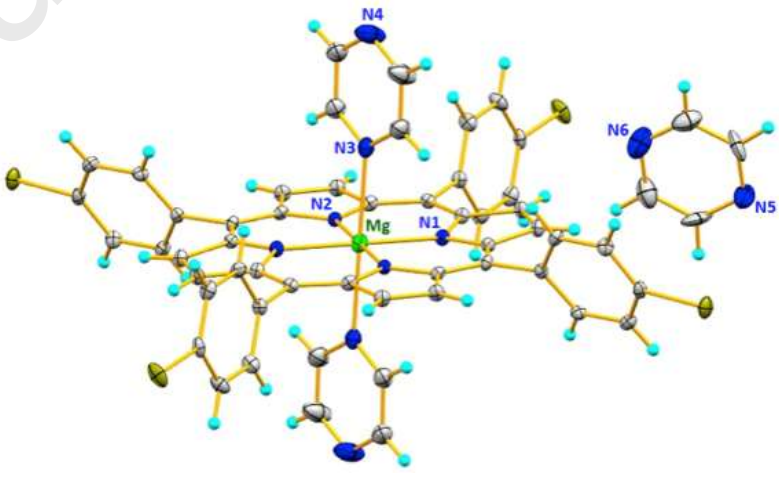

FIGURE 3 ORTEP diagrams of complex **2**; ellipsoids are drawn at the 40%.

Selected structural features for some magnesium porphyrin with axial nitrogen ligand are listed in Table 1. The most important structural feature in these complexes is that the axial Mg-N_{ax} bond for the 4,4'-bpy complex is shorter than those for pyrazine, being 2.143(5) and 2.350(4) Å, respectively (Fig. 4). The axial Mg-N_{ax} bond of [Mg(TPP)(4,4'-bpy)] (**1**), is in good agreement with Mg—N_{ax} bond length (2.143(5) Å) observed in previously studied similar five-coordinate complexes [31,35,37].

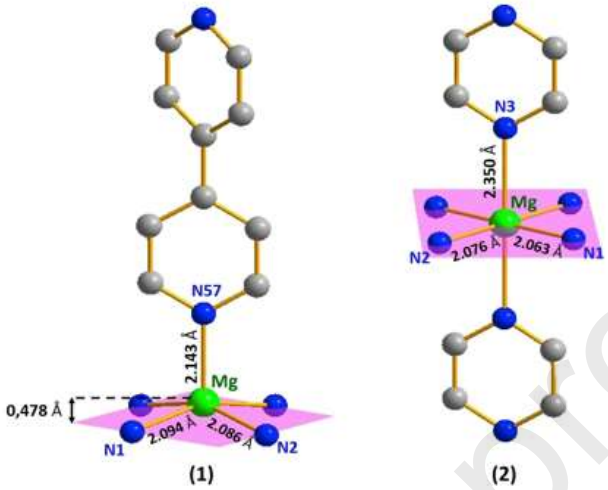

FIGURE 4 Coordination polyhedron of the Mg^{2+} species in complexes **1** (left) and **2**. (right).

Several other examples were reported in the literature for long Mg—N_{ax} bonds in six-coordinate Mg–porphyrin systems. For example, the Mg—N_{ax} bond length in [Mg(TPP)(pip)$_2$] is 2.419(4) Å [34]. For [Mg(TPP)(4-pic)$_2$], [Mg(TPP)(Py)$_2$] and [Mg(OEP)(Py)$_2$], the Mg—N_{ax} bonds are 2.386(4), 2.369(4) and 2.389(2) Å, respectively [33,34,54], which are both very similar to that in [Mg(TBrPP)(pyz)$_2$]. The average Mg–Np bond length for complex **1** is 2.090(3) Å and the displacement of the Mg(II) atom from the mean porphinato core is 0.478 Å. These structural parameters are characteristic of five-coordinate magnesium(II) porphyrins [31,35,59]. For complex **2**, the Mg(II) ion is approximatively in the plane of the porphyrin core, involving a Mg-Np bond (2.070(3) Å) very close to the one in complex **1**; these bonds are consistent with those already reported and obtained for other Mg(II)-porphyrins complexes (see Table 1).

TABLE 1 Selected bond lengths [Å] in several penta and hexa-coordinate magnesium porphyrin complexes.[a]

Compound	M–N_p [b]	M–N_L [c]	Reference
[Mg(TBrPP)(4,4'-bpy)] (**1**)	2.090(3)	2.143(5)	this work
[Mg(TPP)(HIm)]	2.094(2)	2.120(3)	[35]
[Mg(TPP)(N_3)]$^-$	2.1187(16)	1.997(2)	[31]
[Mg(TPP)(NCO)]$^-$	2.1108(15)	2.0471(17)	[31]
[Mg(TPP)(NCS)]$^-$	2.0962(13)	2.0817(15)	[31]
[Mg(TPP)(NCO)]$^-$	2.108(5)	2.055(3)	[37]
[Mg(TBrPP)(pyz)$_2$] (**2**)	2.070(3)	2.350(4)	this work
[Mg(TPBP)(4,4'-bpy)$_2$]	2.065(2)	2.319(3)–2.290(3)	[55]
[Mg(TPP)(1-MeIm)$_2$]	2.071(6)	2.297(8)	[34]
[Mg(TPP)(pip)$_2$]	2.071(3)	2.419(4)	[34]
[Mg(TPP)(4-pic)$_2$]	2.071(3)	2.386(2)	[34]
[Mg(TPP)(py)$_2$]	2.063(2)	2.369(2)	[54]
[Mg(OEP)(py)$_2$]	2.068(2)	2.389(2)	[33]
[Mg(TPBP)(HTMA)$_2$]	2.074(3)	2.438(3)	[36]
[Mg(TPBP)(BABCO)$_2$]	2.066(1)	2.437(1)	[36]

[a] *Distances in [Å];* [b] *Average equatorial metal–nitrogen pyrrole distance;* [c] *Distance between the metal and the nitrogen of the N-donor ligand.*

The 4,4'-bpy ligand in complex **1** is twisted with a dihedral angle of ca. 39.90° between the two pyridyl cycles (Fig. 5), while the values of this dihedral angle in several 4,4'-bpy complexes range between 24° and 46° [60-63]. The values of the dihedral angle between the projection of the plane of the pyridyl group of the 4,4'-bpy axial ligand and the nearest Mg–N_p vector is ca. 40.84°. The two pyrazine planes for the complex **2** are nearly coplanar. The dihedral angle between the plane defined by N1, Mg, and N_{pyz} and the plane of the major pyrazine is 27.05° (Fig. 5). The dihedral angle between the plane of the pyrazine ligand and the 24-atom mean porphyrin plane is 86.05°.

Scheidt and Lee [64] have shown that the porphyrin macrocycle presents four major deformations: (*i*) the ruffling distortion (ruff) is indicated by the values of the *meso*-carbon atoms above and below the porphyrin mean plane; (*ii*) the doming distortion (dom) is often observed in five-coordinate complexes when the axial ligand causes a displacement of the metal center out of the mean plane, and the nitrogen atoms are also displaced toward the axial ligand, (*iii*) the saddle distortion (sad) involves the displacement of the pyrrole rings alternately above and below the mean porphyrin macrocycle so that the pyrrole nitrogen atoms are out of the mean plane, (*iv*) in the waving distortions (wav), the four fragments "(*β*-carbon)-(*α*-carbon)- (*meso*-carbon)-(*α*-carbon)-(*β*-carbon)" are alternatively above and below the 24-atoms of the $C_{20}N_4$ least squares plane (PC plane). Additional quantitative information of two structures are given in Fig. 5, which displays the detailed displacements of each porphyrin core atom (in units of 0.01 Å) from the 24-atom mean planes. The top panels show that porphyrin core of [Mg^{II}(TBrPP)(4,4'-bpy)] (**1**) presents major doming (dom) and comparably small saddle (sad) distortions. Formal diagram of the porphyrinato core of [Mg^{II}(TBrPP)$(pyz)_2$] (**2**) show a quasi-planar conformation of porphyrin macrocycle, the displacement of *meso* and *beta*-carbons from the least-squares plane of $C_{20}N_4$ pophyrinato core are ± 0.012 Å.

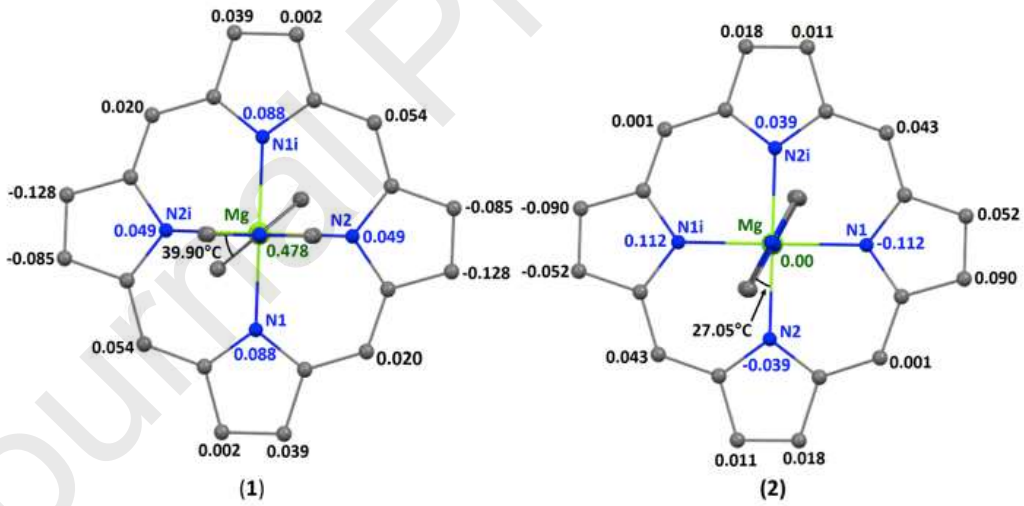

FIGURE 5 Diagram of the porphyrin cores of complexes (**1**) and (**2**) showing the mean plane displacements of the Mg(II) ion and the core atoms shown in Å units and the dihedral angle between the two pyridyl moieties of the 4,4'-bpy molecules and the dihedral angle of the nearest Mg–N_{pyz} vector.

The stability and the cohesion of the free ligand of 4,4'-bpy and the water molecule for the complex **1** are provided by intra-molecular hydrogen bonds and by weak C–H···Cg π interactions (Fig. S15). Starting with the hydrogen bonds, O-H···N and C-H···O type links were evidenced; the oxygen atom of the water molecule acting as both an O–H donor (O1–H1A···N39 and O1–H1B···N32) and a O1 acceptor (C7–H7···O1 and C55–H55···O1) (Table 2 and Fig. S16). The distances between hydrogen and the acceptor atom X (X = O or N) are varying between 1.94 and 2.55 Å. On the other hand, free 4,4'-bpy molecule and porphyrin are linked one to the other by intra-molecular C8–H8···N32 hydrogen bond

(H8···N32 distance range is 2.48 Å). The analysis of the [Mg(TBrPP)(4,4'-bpy)] complex reveals that phenyl rings could form a weak C–Br···Cg π contact (Fig. S16). In this complex there are C–H···Cg π interactions between hydrogen atoms and five-membered pyrrole rings, but also between hydrogen atom and six-membered chelate ring. We find three intermolecular interactions as an H acceptor; two C–H···Cg π interactions involving carbon atoms (C30 and C38) from free 4,4'-bipyridine and the centroids of the pyrrole of the *meso*-porphyrin where five-membered pyrrole rings are H acceptors, and one C2–H2···Cg8 π interaction involving a carbon atom (C2) of pyrrole and the centroid of 4,4'- bipyridine coordinated of neighbouring molecule where six-membered rings are H acceptors (C···Cg vary between 3.549(6) and 3.708(5) Å).

Similarly, the molecular structure and crystal packing for complex **2** (Fig. S17) are stabilised by inter- and intramolecular **C–H···N** hydrogen bond, and by a weak C–H···Cg π interactions (Table 3 and Fig. S18). Remarkably, the free pyrazine nitrogen N5 is linked by intermolecular C16–H16···N5 hydrogen bond with the C16 carbon of the neighbouring porphyrin, and this same free ligand is linked by weak C26–H26···Cg23 π interaction involving a carbon atom (C26) from pyrazine coordinated where six-membered ring for free pyrazine is H acceptors. Neighbouring porphyrins are linked one to the other by weak C18–H18···Cg1 π interaction.

TABLE 2 Inter-and intra-molecular interactions for **1**.

D–H···A	**D–H**	**H···A**	**D···A**	**D–H···A**
O1-H1A...N39 [i]	0.97	1.94	2.890(5)	166
O1-H1B...N32	0.97	2.13	2.967(6)	144
C7-H7...O1	0.95	2.55	3.266(6)	133
C8-H8...N32	0.95	2.48	3.389(6)	159
C55-H55...O1[ii]	0.95	2.50	3.195(6)	130
C–X···Cg (π)		**X···Cg (π)**	**C···Cg (π)**	**C–X···Cg (π)**
C20-Br2...Cg4[iii]		3.7937(16)	4.569(5)	101.18
C20-Br2...Cg24[iv]		3.4629(19)	5.305(5)	160.24
C–H···Cg (π)		**H···Cg (π)**	**C···Cg (π)**	**C–H···Cg (π)**
C2-H2...Cg3 [v]		2.90	3.708(5)	144
C30-H30...Cg2 [vi]		2.93	3.657(6)	134
C38-H38...Cg1 [vi]		2.82	3.549(6)	134

A = acceptor, D = donor, X= heteroatom, Cg = centroid.
Cg1: is the centroid of the N1/C1-C4 *five-membered ring, Cg2: is the centroid of the* N2/C6-C9 *five-membered ring. Cg3:* N39/C38-C40 *six-membered ring, Cg4:* N57/C56-C56 *a six-membered ring. Cg24:* N50/C51-C51 *a six-membered ring.*
Symmetry codes: (i):1-x,-y,-z, (ii): -x,y,-1/2-z; (iii): 1-x,-y,-z; (iv); 1+x,y,z; (v): 1/2+x,1/2+y,z; *(vi):* 1/2-x,1/2-y,-z.

TABLE 3 Inter-and intra-molecular interactions for **2**.

D–H···A	**D–H**	**H···A**	**D···A**	**D–H···A**
C16-H16…N5 [i]	0.93	2.61	3.460(7)	153
C–H···Cg (π)		**H···Cg (π)**	**C···Cg (π)**	**C–H···Cg (π)**
C18-H18…Cg1 [ii]		2.72	3.480(5)	140
C26-H26…Cg23 [iii]		2.95	3.550(6)	123

A = acceptor, D = donor, X= heteroatom, Cg = centroid.
Cg1: is the centroid of the N1/C2-C5 *five-membered ring, Cg23: is the centroid of the* N1/C27-C27 a *six-membered ring. Symmetry codes: (i):* x,1+y,z; *(ii):*-x,1-y,1-z; *(iii):* -x,1+y,1/2-z.

Photophysical properties

Absorption spectroscopy

The UV-Vis absorption spectra of the free base porphyrin base H_2TBrPP, [Mg(TBrPP)] and complexes **1** and **2** recorded in dichloromethane are shown in Fig. 6. The λ_{max} values of these species are listed in Table S4 and compared to

several other *meso*-porphyrins and magnesium metalloporphyrins. The electronic spectra of free base porphyrin contain one intense band around 400 nm (the *Soret* or *B*-band) corresponding to strongly allowed transitions to S2 state, followed by four low intensity absorption bands at 515 nm, 549 nm, 590 nm, and 648 nm attributed to *Q*y (1,0), *Q*y (0,0), *Q*x (1,0) and *Q*x (0,0), respectively (*Q*-bands). When the metal ion was inserted into the porphyrin ring, the number and intensity of the *Q* bands were found to decrease [31, 35, 52], while the intense *Soret* band showed a red shift up to 7 nm (Fig. 6).

According to the literature, the five-coordinated magnesium(II) tetraporphyrin-based complex exhibits an increased *Soret* intensity with slightly red shifted (3-6 nm) *Q*-bands. For the hexa-coordinated Mg-porphyrin analogue, both *Soret* and *Q*-bands are red shift (around 10 nm and 10 to 18 nm, respectively) [65]. Fig. 6 illustrates the UV-visible optical absorption spectral changes observed during the complexation of MgTBrPP with 4,4'-bipyridine or pyrazine ligand. This spectral change is an indication of the formation of new species. Upon addition of the 4,4'-bpy ligand, a marked color variation from purple to blue-green is observed (at concentrations 1.22 10^{-6} mol.L^{-1}). The *Soret* band (427 nm) revealed a larger intensity much than obtained with the individual spectrum of MgTBrPP, while the visible *Q*-bands (565 and 604 nm) were red shifted by 2 nm leading to the formation of new complex 1:1 (4,4'-bpy: complex **1**) binding stoichiometry.

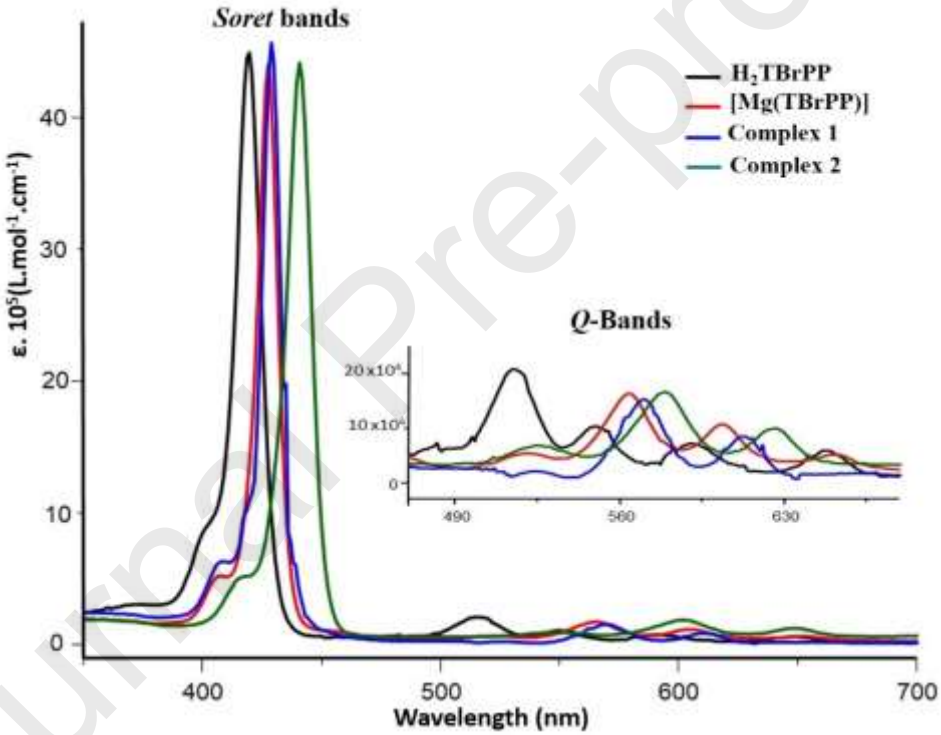

FIGURE 6 UV-vis absorption spectra of H_2TBrPP, [Mg(TBrPP)], [Mg(TBrPP)(4,4'-bpy)] (**1**) and [Mg(TBrPP)$(pyz)_2$] (**2**), in CH_2Cl_2 solution at concentrations around 10^{-6} mol.L^{-1}.

These spectral features are characteristic of a pentacoordinated specie. The important characteristics were consistently observed upon adding an amount of pyrazine to a solution of MgTBrPP. It can be observed (*i*) a marked color variation from purple to blue-green (at concentrations 1.24 10^{-6} mol.L^{-1}), and (*ii*) the red shift of the *Soret* band from 426 nm to 435 nm and the *Q* bands (563 and 603 nm to 578 and 618 nm) indicating transformation to an hexa-coordinated complex. It can also be concluded that the neutral complexes spectra [Mg(TBrPP)(L)] (L = 4,4'-bpy or pyrazine) exhibit larger red shifts of the *Soret* and *Q* bands than those of the anionic complexes of the type [Mg(TPP)(X)], in which X is a pseudo-halide (N_3^-, NCO^-, NCS^-, NCO^-) [31,66] ligand (Table S4).

Spectrofluorometry

Excited-state processes in porphyrins are extremely important for their application in molecular devices. Thus, the fluorescence emission data [67-69] of the porphyrins provide significant information on the singlet excited state properties. The emission spectra of the free base porphyrin, metallo-porphyrin and complexes **1** and **2** are reported in Fig. 7. The values of fluorescence quantum yields (Φ_f) of these synthesized complexes were measured in dichloromethane, using MgTPP as reference (Φ_f = 0.15) [31,70] and are summarized in Table S5.

As previously reported, upon excitation at 420 nm the free base porphyrin H_2TBrPP exhibit two emission bands at 654 and 720 nm [35] corresponding to *Q* (0,0) and *Q* (0,1) transitions, respectively, the intensity of the *Q* (0,0) being higher than the *Q* (0,1) transition (Fig. S19 a). The spectra is typical of many free-base porphyrins [36,68,69]. The major emission peaks for [Mg(TBrPP)] appear at 612 and 660 nm for *Q* (0,0) and *Q* (0.1) bands, respectively, upon excitation at 427 nm (Fig. S19b). As shown in Table S4 and Fig. 7, the main impact of the magnesium insertion resides in the large blue shift (~ 42 nm) for the strongest emission band *Q* (0,0) and ~ 60 nm for the second band *Q* (0,1). The axially ligated metallo-porphyrins (complexes **1** and **2**) results in two emission bands (from S2 excited state to fundamental state S0) centered at 613 nm (S2 [*Q* (0,0)] to S0) and 660 nm (S2 [*Q* (0,1)] to S0) for complex **1** when excited at 429 nm, and at 612 nm (S2 [*Q* (0,0)] to S0) and 663 nm (S2 [*Q* (0,1)] to S0) for complex **2** when excited at 434 nm (Figs. S19c and d).

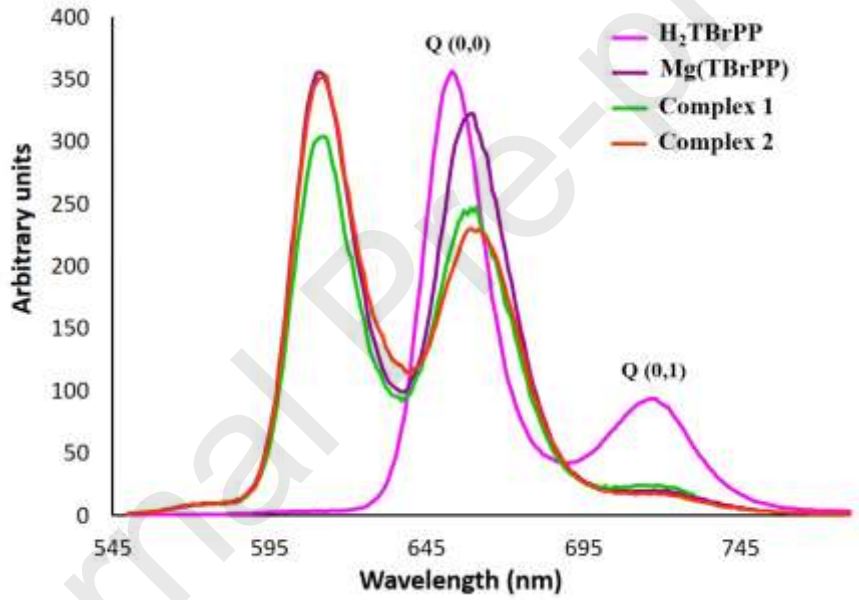

FIGURE 7 Emission spectra of H_2TBrPP (λ_{exc} = 420 nm) , Mg(TBrPP) (λ_{exc} = 427 nm), complexes **1** (λ_{exc} = 429 nm) and **2** (λ_{exc} = 434 nm) in a 10^{-6} mol.L^{-1} dichloromethane solution.

These bands exhibit similar behaviour to [Mg(TBrPP)] (Fig. S19) and to those already reported in the literature for [Mg^{II}(TPP)$(THF)_2$] [71] and [Mg^{II}(TPP)(NCO)]$^-$ [37] for example. In the 350–700 nm spectral range, the excitation spectra are similar to the absorption spectra, indicating that it corresponds to similar electron transition process (Fig. S19). The fluorescence quantum yields (Φ_f) of H_2TBrPP, [Mg^{II}(TBrPP)] and for the obtained complexes are in the range 0.050 - 0.065; these values do not depend on the nature of the axial ligand, but they depend more largely on the nature of the phenyl substitution in the *meso* position, that is to say, compounds including heavy atom such as bromine, reduces fluorescence quantum yield (see Table S5).

Biological Studies

Antioxidant activity of complexes 1 and 2 by DPPH radical scavenging method

1,1-diphenyl-2-picrylhydrazyl (DPPH) radical assay is a simple, rapid and suitable method extensively used to assess the antioxidant properties of compounds. The quite stable DPPH nitrogen centered radical posseses a characteristic absorption which decreases when exposed to antioxidants [72]. It reacts with hydrogen donating functions resulting in a colour change from purple to yellow. The intensity of this phenomena is related to the number of captured electrons [73], *i.e.*, the greater the free radical scavenging capacity of an antioxidant compounds, the more reduction of DPPH and the less purple colour of the sample.

In the present study, the scavenging activity of the free base porphyrin base H_2TBrPP, Mg(TBrPP), [Mg(TBrPP)(4,4'-bpy)] (**1**), and [Mg(TBrPP)(pyz)$_2$] (**2**) against DPPH were evaluated at different concentrations (in a range comparable to usual literature assays) from 25 to 100 µg/mL (*i.e.* from approximatively 10^{-5} to 10^{-4} M). The antioxidant activity efficiency is quantified and reported Fig. 8.

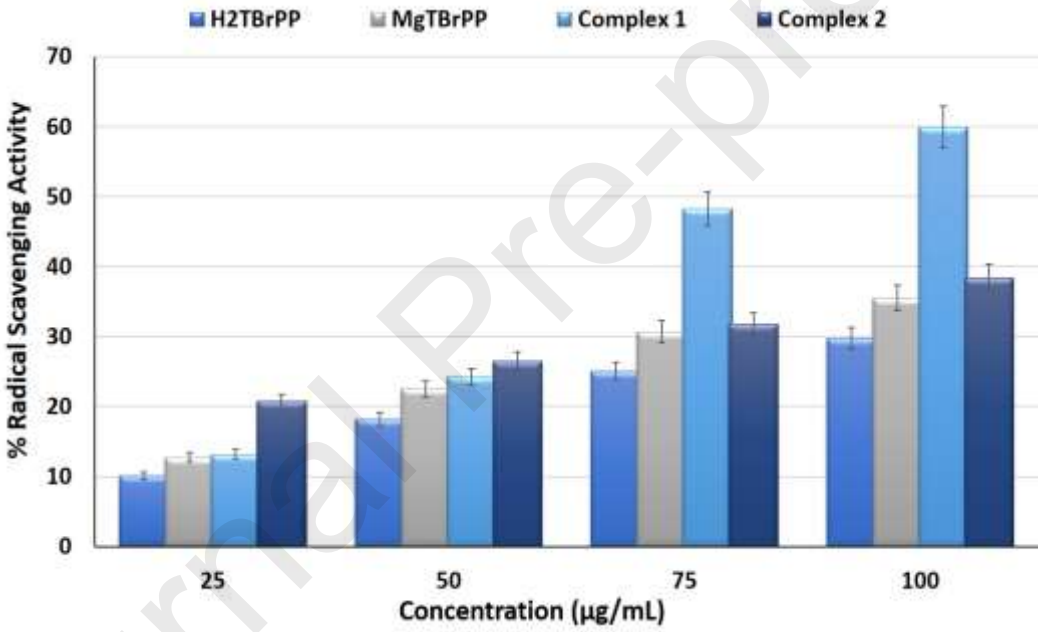

FIGURE 8 Emission DPPH radical scavenging activity of H_2TBrPP, Mg(TBrPP), complexes **1** and **2**.

As expected, free radical scavenging activity of these complexes was concentration dependent. Free radical scavenging rate increases with increasing concentration of the inclusion compound solution. The highest antioxidant activity was obtained for Mg-porphyrin compounds with respect to H_2TBrPP free base porphyrin. Axial ligand presence affects also antioxidant activity. As shown Fig. 8, the amount of DPPH radical of the complex **1** at the concentration of 25 and 50 µg/mL was found to be 13% and 24%, respectively, which was slightly weaker than for complex **2** (20% and 25%) at the same concentrations. However, at 100 µg/mL, the DPPH scavenging activity of [Mg(TBrPP)(4,4'-bpy)] (**1**) reached 60%, which was significantly higher than that of [Mg(TBrPP)(pyz)$_2$] (**2**) (40%) at the same concentration. These results confirm previous reports from Ferruzzi *et al.* [74] and Endo *et al.* [75] who determined *in vitro* the antioxidant activity of natural chlorophyll derivatives. They evidenced that the magnesium might alter the electron-donating ability from the conjugated porphyrin system, which strengthen the apparent antioxidant activity of chlorophylls. By comparison with already well-known antioxidants, our new complexes remained a little bit less active in the same range of

concentration. As far as radical scavenging activity is concerned and at a concentration of 100 µg/mL, Vitamin C (Vit C) and Butylated Hydroxy-Toluene (BHT) for example reach approximatively 80 and 70%, respectively [76,77]. As already inspected and mentioned in the literature [78], the radical scavenging activity (and related prevention of oxidative damage) is correlated to the standard reduction potential (E°) of the species; this one can be finely tuned with the nature of the surrounding ligands (E°') in order to adapt the best to the E° values of ROS of interest. We assume this study is original illustration of this point.

Antifungal Activity

The antifungal activities of the free base porphyrin H_2TBrPP, Mg(TBrPP), [Mg(TBrPP)(4,4'-bpy)] (**1**) and [Mg(TBrPP)(pyz)$_2$] (**2**) were quantitatively assessed by the presence, or absence of inhibition zones against three yeasts strains (*C. krusei* ATCC6258, *C. albicans* ATCC90028 and *C. neoformans* ATCC14116) and two fungal strains (*A. brasiliensis* ATCC16404 and *A. fumigatus* ATCC204305). The diameters of inhibition zones observed with the well diff usion method are shown in Fig. 9.

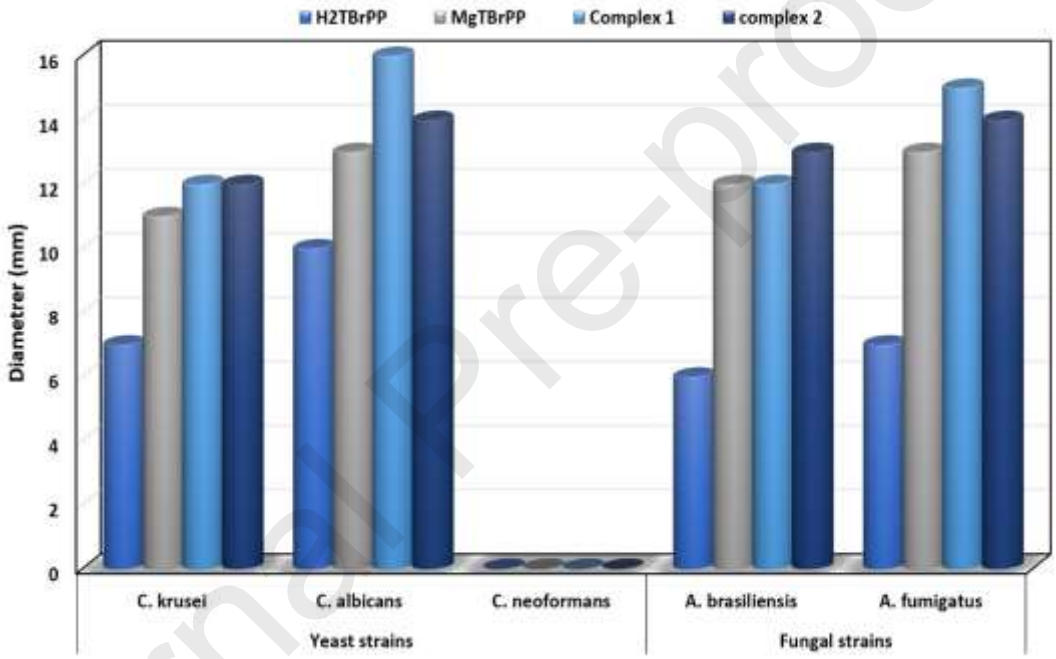

FIGURE 9 *In vitro* antifungal activity of H_2TBrPP, Mg(TBrPP), [Mg(TBrPP)(4,4'-bpy)] (**1**) and [Mg(TBrPP)(pyz)$_2$] (**2**) at concentrations around 10^{-3} mol.L^{-1}

Porphyrin derivatives have been reported to possess significant antifungal activity [79,80]. We synthesized analogues in an attempt to find newer and better antifungal agents. In the present research work, several compounds were evaluated for antifungal activity. The results reveal that the yeasts strain *C. albicans* was the most sensitive and the strain *C. neoformans* was the most resistant. In fact, no zone of inhibition was observed for our compounds on this yeast strain (Fig. 9). Based on zones of inhibition results, the lowest activity is observed for the free base porphyrin H_2TBrPP. Contrariwise, the Mg(TBrPP), starting material and complexes **1** and **2** displayed nearly the same zones of inhibitions against all strains (yeasts and fungal). These magnesium derivatives showed a zone inhibition diameter between 13 and 16 mm and of 11 to 12 mm against *C. albicans* and *C. krusei*, respectively. They also inhibited *A. brasiliensis* (12 - 13 mm) and *A. fumigatus* (13 - 15 mm). These complexes exhibit less antifungal activity than the standard drug Nystatin [81], who owns 29 and 19 mm in diameter of zone inhibition against *C. albicans* and *A. fumigatus*, respectively. The literature survey revealed that antifungal activity of these magnesium complexes was comparable and in some cases even superior, to previously synthesized and studied metalloporphyrins. For example, Singh *et al.* [81], synthesized tetra-

porphyrins derivatives [M: 2H, Cu(II), Co(II), Ni(II)] and investigated their antifungal properties. According to the results these complexes produced diameters of zones of inhibition between 15 mm and 22 mm against *C. albicans* and between 10 mm and 19 mm against *A. fumigatus*. Moreover, our complexes are slightly more active than Mn(III) and Co(II)-based porphyrins derivatives reported by Karimipour *et al.* (*A. fumigatus* between 9 mm and 11 mm) [82] but remain in the same principles explaining the activity increase for the metal complexes [83-85]. According to the Overtone's concept for cell permeability [83,84] and due to the liphophilicity as an important factor in controling the antifungal activity , the lipid membrane surrounding the cell, favours the passage of only the lipid-soluble materials. Tweedy's chelation theory [85] shows that the polarity of the metal ion will be reduced to a greater extent due to overlap of the porphyrin orbital and partial sharing of the positive charge of the metal ion with donor group. However, in Mg-porphyrin compounds, Mg(II) is almost completely neutralized by the porphyrin. Therefore, the polarity is minimized and the lipo-solubility of Mg-porphyrin compounds are significantly increased. This increase in lipophilicity enhances the penetration of the complexes into lipid membranes and disturb the respiration process of the cell. In this study, Mg-porphyrin compounds were more reactive than the non-metallateded H_2TBrPP porphyrin ligand.

CONCLUSION

In the present work, two new magnesium(II) porphyrin complexes, [Mg(TBrPP)(4,4'-bpy)] (**1**) and [Mg(TBrPP)(pyz)$_2$] (**2**) have been prepared and characterized in solution and at the solid state (X-ray diffraction structures). The UV-visible spectrum of these latter exhibits red-shifted *Soret* band compared to the [Mg(TBrPP)]. The fluorescence data are very similar to those of already reported magnesium porphyrin complexes. The single crystal molecular structures show clearly that: (*i*) the five-coordinate species **1** involving one molecule of the complex [Mg(TBrPP)(4,4'-bpy)], two free 4,4'-bipyridine ligand and two water molecule linked together by O–H···N, C–H···O and C–H···N hydrogen bonds and C-H···π interactions., (*ii*) the six-coordinate species **2** comprised by one molecule of the complex [Mg(TBrPP)(pyz)$_2$] (**2**) and one free pyrazine ligand which are linked together by hydrogen bonds of C–H···N type and C–H···π interactions. For quite concentrated solution (NMR), compounds **1** and **2** seem to lead to low energy bonds-based polymeric species The biological studies reveal that the magnesium complexes may be a good candidate as antioxidant and antifungal agent, especially the [Mg(TBrPP)(4,4'-bpy)] complex (**1**, involving the most stable Mg-N_L axial bond), which is the most active one. Indeed, these complexes present a high antioxidant activity according to the DPPH assay. The biological activities obtained from present work could be helpful to design and develop new efficient biological and therapeutic agents.

Acknowledgements N.A. thanks The Tunisian Ministry of Higher Education and Scientific Research for the financial support.

REFERENCES

1. M. Teraguchi, N. Nahata, T. Nishimura, T. Aoki, T. Kaneko, Helix-Sense-Selective Polymerization of Phenylacetylenes Having a Porphyrin and a Zinc-Porphyrin Group: One-Handed Helical Arrangement of Porphyrin Pendants, Polymers 11 (2019) 274.
2. S. Praban, P. Piromjitpong, V. Balasanthiran, S. Jayaraj, M.H. Chisholm, J. Tantirungrotechai, K. Phomphrai, Highly efficient metal(iii) porphyrin and salen complexes for the polymerization of rac-lactide under ambient conditions, Dalton Trans. 48 (2019) 3223-3230.

3. Z. Wei, D. Zhang, C. Li, L. Bai, H. Liu, H. Yan, Preparation of an iron porphyrin-based polymer monolithic column via atom transfer radical polymerization for the separation of proteins and small molecules, Anal. Methods **9** (2017) 2596-2602.
4. O.J. Fakayode, E.H.M. Sakho, S.P. Songca, O.S. Oluwafemi,MRS Communications 1 (2019).
5. A.N. Gupta, K. Neupane, N. Rezajooei, L.M. Cortez, V.L. Sim, M.T. Woodside, Pharmacological chaperone reshapes the energy landscape for folding and aggregation of the prion protein, Nat. Commun. **7** (2016) 12058.
6. E.Yu. Tyulyaeva, Modern Approaches in the Synthesis of Noble Metal Porphyrins for Their Practical Application (Review), Russ. J. Inorg. Chem. 64 (2019) 1775–1802.
7. C. Farley, A. Aggarwal, S. Singh, A. Dolor, P. To, A. Falber, M. Crossley, C.M. Drain, A Structural Model of Nitro-Porphyrin Dyes Based on Spectroscopy and Density Functional Theory, J. Comput. Chem. 39 (2018) 1129-1142.
8. M. Bagherzadeh, E. Mesbahi, J. Porphyr. Phthalocyanines 22 (2018) 1–9.
9. S. Zakavi, A.H. Amiri, F. Asadi, Axial base-controlled catalytic activity, oxidative stability and product selectivity of water-insoluble manganese and iron porphyrins for oxidation of styrenes in water under green conditions, Appl Organometal Chem. 32 (2018) 4117.
10. V.S.d. Silva, W. C.d.S. Vieira, A.M. Meireles, G.M. Ucoski, S. Nakagaki, Y.M. Idemoria, G. DeFreitas-Silva, Biomimetic oxidation of cyclic and linear alkanes: high alcohol selectivity promoted by a novel manganese porphyrin catalyst, New J.Chem., 41 (2017) 997-1006.
11. F. Teixeira, M.N.D.S. Cordeiro, Strengths, Weaknesses, Opportunities and Threats: Computational Studies of Mn- and Fe-Catalyzed Epoxidations, Catalysts **7** (2017) 2.
12. L. Cuesta-Aluja, A.M. Masdeu-Bulto, Iron(III) Versatile Catalysts for Cycloaddition of CO2 to Epoxides and Epoxidation of Alkenes, ChemistrySelect 1 (2016) 2065–2070.
13. G. Huang, Y. Liu, J.L. Cai, X.F. Chen, S.K. Zhao, Y.A. Guo, S.J. Wei, X. Li, Heterogeneous biomimetic catalysis using iron porphyrin for cyclohexane oxidation promoted by chitosan , Appl. Surf. Sci. 402 (2017) 436–443.
14. I. Bernar, F.P.J.T. Rutjes, J.A.A.W. Elemans, R.J.M. Nolte, Aerobic Epoxidation of Low-Molecular-Weight and Polymeric Olefins by a Supramolecular Manganese Porphyrin Catalyst, Catalysts 9 (2019) 195.
15. Z.Y. Hou, W. Dehaen, J. Lyskawa, P. Woiselc, R. Hoogenboom, , Chem. Commun. 00 (2016) 1-3.
16. I.A. Abdulaeva, K.P. Birin, A.B. Lemeune, A. Yu. Tsivadze, Y.G. Gorbunova, Heterocycle-appended porphyrins: synthesis and challenges, Coord. Chem. Rev. 407 (2020) 213108.
17. M.D. Peeks, C.E. Tait, P. Neuhaus, G.M. Fischer, M. Hoffmann, R. Haver, A. Cnossen, J.R. Harmer, C.R. Timmel, H.L. Anderson, Electronic Delocalization in the Radical Cations of Porphyrin Oligomer Molecular Wires, J. Am. Chem. Soc. 139 (2017) 10461−10471.
18. R. Paolesse, S. Nardis, D. Monti, M. Stefanelli, C.D. Natale, Porphyrinoids for Chemical Sensor Applications, Chem. Rev. 117 (2017) 2517−2583.
19. D. Khusnutdinova, A.M. Beiler, B.L. Wadsworth, S.I. Jacob, G.F. Moore, Metalloporphyrin-modified semiconductors for solar fuel production, Chem. Sci. 8 (2017) 253-259.
20. A.J. Stasyuk, O.A. Stasyuk, M. Solà, A.A. Voityuk, Expeditious Preparation of Open-Cage Fullerenes by Rhodium(I)-Catalyzed [2+2+2] Cycloaddition of Diynes and C60: an Experimental and Theoretical Study, Chem. Eur. J. 24 (2018) 10653-10661.
21. Y. Fan, B. Feng, Y. Huang, X. Lu, Investigation of the Electron Transfer between Levodopa and Zinc Porphyrins at Bionic Interface, Int. J. Electrochem. Sci. 13 (2018) 3382–3395.

22. Ö. Birel, S. Nadeem, H. Duman, Porphyrin-Based Dye-Sensitized Solar Cells (DSSCs): a Review, J. Fluoresc. 27 (2017) 1075-1085.
23. A.Yu. Tsivadze, A.Yu. Chernyad'ev, Metal Crown-Porphyrin Complexes: Preparation, Optical Properties, and Applications (Review), Russ. J. Inorg. Chem. 65 (2020)1662–1686.
24. C. Decker, H. Schubert, S. May, A. Fahr, Pharmacokinetics of temoporfin-loaded liposome formulations: Correlation of liposome and temoporfin blood concentration, J Control Release 166 (2013) 277–285.
25. J. Kou, D. Dou, L. Yang, Porphyrin photosensitizers in photodynamic therapy and its applications, Oncotarget 8 (2017) 81591-81603.
26. K.D. Borah, J. Bhuyan, Magnesium porphyrins with relevance to chlorophylls, Dalton Trans. 46 (2017) 6497-6509.
27. M.E. El-Khouly, Y. Araki, O. Ito, S. Gadde, A.L. McCarty, P.A. Karr, M.E. Zandler, F. D'Souza, Spectral, electrochemical, and photophysical studies of a magnesium porphyrin–fullerene dyad, Phys. Chem. Chem. Phys. 7 (2005) 3163–3171.
28. F. D'Souza, M.E. El-Khouly, S. Gadde, A.L. McCarty, P.A. Karr, M.E. Zandler, Y. Araki, O. Ito, Self-Assembled via Axial Coordination Magnesium Porphyrin−Imidazole Appended Fullerene Dyad: Spectroscopic, Electrochemical, Computational, and Photochemical Studies, J. Phys. Chem. B 109 (2005) 10107-10114.
29. N.F. Goldshleger, M.A. Lapshina, V.E. Baulin, A.A. Shiryaev, Yu. G. Gorbunova, A. Yu. Tsivadze, Supramolecular assemblies based on crown- and phosphoryl-substituted phthalocyanines and their metal complexes in microheterogeneous media, Russ. Chem. Bull., Int. Ed. 69 (2020) 1223—1244.
30. (a) R. Timkovich, A. Tulinsky, The Structure of Aquomagnesium Tetraphenylporphyrin, J. Am. Chem. Soc. 91 (1969) 4430-4432; (b) H.S. Chow, R. Serline, C.E. Strouse, The Crystal and Molecular Structure and Absolute Configuration of Ethyl Chlorophyllide a Dihydrate. A Model for the Different Spectral Forms of Chlorophyll a, J. Am. Chem. Soc. 97 (1975) 7230-7237.
31. K. Ezzayani, Z. Denden, S. Najmudin, C. Bonifácio, E. Saint-Aman, F. Loiseau, H. Nasri, Exploring the Effects of Axial Pseudohalide Ligands on the Photophysical and Cyclic Voltammetry Properties and Molecular Structures of Mg(II) Tetraphenyl/porphyrin Complexes, Eur. J. Inorg. Chem. 31 (2014) 5348-5361.
32. N. Amiri, S. Nasri, T. Roisnel, G. Simonneaux, H. Nasri, Crystal structure of di-aqua-[5,10,15,20-tetra-kis-(4-bromo-phen-yl)porphyrinato-N]magnesium, Acta. Cryst. E. 71 (2015) 73-74.
33. R. Bonnett, M.B. Hursthouse, M.K.M. Abdul, B.J. Mateen, J. *Chem. Soc.,* Perkin Trans. 2 (1977) 2072.
34. V. McKee, C.C. Ong, G.A. Rodley, X-ray Crystal and Molecular Structures of Related Octahedral Magnesium Tetraphenylporphyrin Complexes, Inorg. Chem. 23 (1984) 4242-4248.
35. N. Amiri, F.B. Taheur, S. Chevreux, E. Wenger, G. Lemercier, H. Nasri, Synthesis, crystal structure and spectroscopic characterizations of porphyrin-based Mg(II) complexes – Potential application as antibacterial agent, Tetrahedron 73 (2017) 7011-7016.
36. N. Amiri, M. Hajji, F.B. Taheur, S. Chevreux, T. Roisnel, G. Lemercier, H. Nasri, Two novel magnesium(II) meso-tetraphenylporphyrin-based coordination complexes: Syntheses, combined experimental and theoretical structures elucidation, spectroscopy, photophysical properties and antibacterial activity, J. Solid State Chem. 258 (2018) 477–484.
37. K. Ezzayani, A.B. Khelifa, E. Saint-Aman, F. Loiseau, H. Nasri, Synthesis, spectroscopic characterizations, cyclic voltammetry investigation and molecular structure of the di-μ-cyanato-N-bis(μ-1,4,7,10,13,16-hexaoxacyclooctadecane)bis(5,10,15,20-tetraphenylporphyrinato)dimagnesiumdipotassium complex, Polyhedron 117 (2016) 817-825.

38. S.A. Ikbal, S. Brahma, S.P. Rath, Building-up Remarkably Stable Magnesium Porphyrin Polymers Self-Assembled via Bidentate Axial Ligands: Synthesis, Structure, Surface Morphology, and Effect of Bridging Ligands, Inorg. Chem. 51 (2012) 9666-9676.
39. J. Bhuyan, S. Sarkar, Self-Assembly of Magnesium and Zinc Trimethoxyphenylporphyrin Polymer as Nanospheres and Nanorods, Cryst. Growth Des. 11 (2011) 5410-5414.
40. S. Campestrini, U. Tonellato, Manganeseporphyrin-catalysed heterogeneous and unusually chemioselective oxidations of sulfides by monopersulfate in supercritical CO_2, J. Mol. Catal. A: Chem. 164 (2000) 263.
41. P. Hoffmann, G. Labat, A. Robert, B. Meunier, Highly Selective Bromination of Tetramesitylporphyrin: An Easy Access to Robust Metalloporphyrins, M-Br8TMP and M-Br8TMPS. Examples of application in catalytic oxygenation and oxidation reactions, Tetrahedron Lett. (1990) 31, 1991
42. P. Bhyrappa, B. Purushothaman, Perbrominated 2-nitrotetraphenylporphyrins: electrochemical and axial ligation properties, J. Chem. Soc., Perkin Trans. 2 (2001) 238-242.
43. F. D'Souza, A. Villard, E. Van Caemelbecke, M. Franzen, T. Boschi, P. Tagliatesta, K. M. Kadish, Electrochemical and Spectroelectrochemical Behavior of Cobalt(III), Cobalt(II), and Cobalt(I) Complexes of meso- etraphenylporphyrinate Bearing Bromides on the β-Pyrrole Positions, Inorg. Chem., 32 (1993) 4042-4048.
44. R. Kachadourian, M. M. Flaherty, L. C. Alvin, M. Patel, B. J. Day, Synthesis and in vitro antioxidant properties of manganese(III) β-octabromo-meso-tetrakis(4-carboxyphenyl)porphyrin, J. Inorg. Biochem., 95 (2003) 240-248.
45. Yu.B. Ivanova, N.V. Chizhova,N.Zh. Mamardashvili, Synthesis and Spectral and Coordination Properties of Perhalogenated Tetraphenylporphyrins, Russ. J. Gen. Chem. 90 (2020) 2098–2104.
46. S. Dhifaoui, S. Nasri, G. Gontard, A.C. Ghosh, Y. Garcia, C. Bonifácio, S. Najmudin, V. Marvaud, H. Nasri, Synthesis, Mössbauer, Cyclic voltammetry, Magnetic properties and Molecular Structures of the Low-spin iron(III) Bis(pyrazine) Complexes with the para-fluoro and para-chloro substituted meso-tetraphenylporphyrin, Inorganica Chim. Acta 477 (2018) 114-121
47. A. Altomare, M.C. Burla, M. Camalli, G.L. Cascarano, C. Giacovazzo, A. Guagliardi, A.G.G. Moliterni, G. Polidori, R. Spagna, SIR97: a new tool for crystal structure determination and refinement, J. Appl. Cryst. 32 (1999) 115-119.
48. G.M. Sheldrick, Crystal structure refinement with SHELXL, Acta Cryst. C71 (2015) 3-8.
49. SADABS, Bruker AXS Inc., Madison, Wisconsin, USA, (2012).
50. D.D. Perrin, W.L.F. Armarego, Purification of Organic Solvents, Pergamon Press, Oxford, (1988).
51. A.D. Adler, F.R. Longo, J.D. Finarelli, J. Goldmacher, J. Assour, L. Korsakoff, A Simplified Synthesis for meso-Tetraphenylporphin, J. Org. Chem. 32 (1967) 476-476.
52. J.S. Lindsey, N.J. Woodford, A Simple Method for Preparing Magnesium Porphyrins, Inorg. Chem. 34 (1995) 1063-1069.
53. L.J. Boucher, J.J.J. Katz, The Infared Spectra of Metalloporphyrins (4000-160 Cm^{-1}), Am. Chem. Soc. 89 (1967) 1340–1345.
54. G. Wu, A. Wong, S. Wang, Solid-state ^{25}Mg NMR, X-ray crystallographic, and quantum mechanical study of bis(pyridine)-(5,10,15,20-tetraphenyl porphyrinato)magnesium(II), Can. J. Chem. 81 (2003) 275–283.
55. N. Amiri, M. Hajji, T. Roisnel, G. Simonneaux, H. Nasri, Synthesis, molecular structure, photophysical properties and spectroscopic characterization of new 1D-magnesium(II) porphyrin-based coordination polymer, Res Chem Intermed. 44 (2018) 5583–5595.

56. R. Soury, M. Jabli, T.A. Saleh, W.S. Abdul-Hassan, E. Saint-Aman, F. Loiseau, C. Philouze, H. Nasri, Tetrakis(ethyl-4(4-butyryl)oxyphenyl)porphyrinato zinc complexes with 4,4′-bpyridin: synthesis, characterization, and its catalytic degradation of Calmagite, RSC Adv. 8 (2018) 20143–20156.
57. S. Nasri, I. Zahou, I. Turowska-Tyrk, T. Roisnel, F. Loiseau, E. Saint-Amant, H. Nasri, Synthesis, Electronic Spectroscopy, Cyclic Voltammetry, Photophysics, Electrical Properties and X-ray Molecular Structures of meso-{Tetrakis[4-(benzoyloxy)phenyl]porphyrinato}zinc(II) Complexes with Aza Ligands, Eur. J. Inorg. Chem. 31 (2016) 5004–5019.
58. R. Soury, M. Jabli, T.A. Saleh, W.S. Abdul-Hassan, E. Saint-Aman, F. Loiseau, C. Philouze, A. Bujacz, H. Nasri, Synthesis of the (4,4′-bipyridine)(5,10,15,20-tetratolylphenylporphyrinato)zinc(II) bis(4,4-bipyridine) disolvate dehydrate and evaluation of its interaction with organic dyes, Journa of Molecular Liquids 264 (2018) 134–142.
59. J. Bhuyan, R. Sarkar, S. Sarkar, A Magnesium Porphyrin Bicarbonate Complex with CO_2-Modulated Photosystem I Action, Angew. Chem. Int. Ed. 50 (2011) 10603-10607.
60. A. Mansour, M. Zaied, I. Ali, S. Soliman, M. Othmani, Synthesis, molecular structure, spectroscopic characterization and antibacterial activity of the Co(III) (chlorido)(pyridine) and (chlorido)(4,4′-bipyridine) “picket fence” porphyrin complexes, Polyhedron 127 (2017) 496-504.
61. A. Mansour, Y. Belghith, M.S. Belkhiria, A. Bujaczb, V. Guérineau, H. Nasri, Synthesis, crystal structures and spectroscopic characterization of Co(II) bis(4,4′-bipyridine) with meso-porphyrins αβαβ-tetrakis(o-pivalamidophenyl) porphyrin (αβαβ-TpivPP) and tetraphenylporphyrin (TPP), J. Porphyrins Phthalocyanines 17 (2013) 1094-1103.
62. A.D. Shukla, P.C. Dave, E. Suresh, A. Das, P. Dastidar, Multicomponent Zn-tetraphenylporphyrins: syntheses, characterization and their self assembly in the solid state, Chem. Soc., Dalton Trans. **0** (2000) 4459-4463.
63. A. Fidalgo-Marijuan, G. Barandika, B. Bazan, M.K. Urtiaga, L. Lezama, M.I. Arriortua, Fe–TPP Coordination Network with Metalloporphyrinic Neutral Radicals and Face-to-Face and Edge-to-Face π–π Stacking, Inorg. Chem. 52 (2013) 8074-8081.
64. W.R. Scheidt, Y. Lee, Recent advances in the stereochemistry of metallotetrapyrroles, Struct. Bonding 64 (1987) 1–70.
65. (a) J.R. Miller, G.D. Dorough, Pyridinate Complexes of Some Metallo-derivatives of Tetraphenylporphine and Tetraphenylchlorin, J. Am. Chem. Soc. 74 (1952) 3977-3981. (b) K.M. Kadish, L.R. Shiue, Investigation of the Axial Ligand Binding Reactions of (meso-Tetraphenylporphinato)magnesium(II) with Nitrogenous Bases, Inorg. Chem. 21 (1982) 1112-1115.
66. L. Jiang, R.A. Zaenglein, J.T. Engle, C. Mittal, C.S. Hartley, C.J. Ziegler, H. Wang, Water-soluble ionic benzoporphyrins, Chem. Commun. 48 (2012) 6927–6929.
67. C. Timiriazeff, Colourless Chlorophyll, Nature 32 (1885) 342.
68. J.P. Strachan, S. Gentemann, J. Seth, W.A. Kalsbeck, J.S. Lindsey, D. Holten, D.F. Bocian, Effects of Orbital Ordering on Electronic Communication in Multiporphyrin Arrays, J. Am. Chem. Soc. 119 (1997) 11191–11201.
69. J. Zhang, P. Zhang, Z. Zhang, X.J. Wei, Spectroscopic and Kinetic Studies of Photochemical Reaction of Magnesium Tetraphenylporphyrin with Oxygen, J. Phys. Chem. A 113 (2009) 5367–5374.
70. M. Gouterman, Spectra of porphyrins, J. Mol. Spectrosc. 6 (1961) 138-163.
71. E.J. Shin, D. Kim, Substituent effect on the fluorescence quenching of various tetraphenylporphyrins by ruthenium tris(2,2′-bipyridine) complex, J. Photochem. Photobiol. A: Chem. 152 (2002) 25-31.
72. R. Thangam, V. Suresh, S. Kannan, Optimized extraction of polysaccharides from Cymbopogon citratus and its biological activities, Int. J. Biol. Macromol. 65 (2014) 415–423.

73. Y. Carmona-Jimenez, M.V. Garcia-Moreno, J.M. Igartuburu, C.G. Barroso, Simplification of the DPPH assay for estimating the antioxidant activity of wine and wine by-products, Food Chem. 165 (2014) 198–204.
74. M.G. Ferruzzi, V. Böhm, P.D. Courtney, S.J. Schwartz, Antioxidant and Antimutagenic Activity of Dietary Chlorophyll Derivatives Determined by Radical Scavenging and Bacterial Reverse Mutagenesis Assays, J. Food Sci. 6 (2002) 2589–2595.
75. Y. Endo, R. Usukï, T. Kaneda, Antioxidant effects of chlorophyll and pheophytin on the autoxidation of oils in the dark. II. The mechanism of antioxidative action of chlorophyll, J Am Oil Chem Soc. 62 (1985) 1387–1390.
76. W.-L. Chu, Y.-W. Lim, A.K. Radhakrishnan, P.-E. Lim, Protective effect of aqueous extract from Spirulina platensis against cell death induced by free radicals, BMC Complement Altern. Med. 10 (2010).
77. P. Hashemi, F. Mohagheghi, M.R. Bigdeli, B. Rasoulian, M.R. Pour, The neuroprotective effect of olive leaf extract is related to improved blood–brain barrier permeability and brain edema in rat with experimental focal cerebral ischemia, Phytomedicine 18 (2011) 170–175
78. M.Baranowska, K. Suliborsk, W. Chrzanowski, B. Kusznierewicz, J. Namieśnik, A. Bartoszek, The relationship between standard reduction potentials of catechins and biological activities involved in redox control, Redox Biology 17 (2018) 355-366.
79. S. Moghnie, A. Tovmasyan, J. Craik, I. Batinic-Haberle, L. Benov, Cationic amphiphilic Zn-porphyrin with high antifungal photodynamic potency, Photochem. Photobiol. Sci. 16 (2017) 1709-1716.
80. G.D. Bajju, S. Kundan, M. Bhagat, D. Gupta, A. Kapahi, G. Devi, Synthesis and spectroscopic and biological activities of Zn(II) porphyrin with oxygen donors, Bioinorgan. Chem. Appl. 2014; 1-13.
81. U. Singh, A.M. Malla, I.A. Bhat, A. Ahmad, M.N. Bukhari, S. Bhat, S. Anayutullah, A.A. Hashmi, Synthesis, molecular docking and evaluation of antifungal activity of Ni(II),Co(II) and Cu(II) complexes of porphyrin core macromolecular ligand, Microb Pathog. 93 (2016) 172-179.
82. G. Karimipour, S. Kowkabi, A. Naghiha, New aminoporphyrins bearing urea derivative substituents: synthesis, characterization, antibacterial and antifungal activity, Braz. Arch. Biol. Technol. 58 (2015) 431-442.
83. N. Dharamraj, P. Viswanathamurthi, K. Natarajan, Ruthenium(II) complexes containing bidentate Schiff bases and their antifungal activityd, Trans Met Chem. 26 (2001) 105-109.
84. C. Zhuang, X. Tang, D. Wang, A. Xia, W. Lian, Y. Shi, T. Shi, An unsymmetrical porphyrin and its metal complexes: Synthesis, spectroscopy, thermal analysis and liquid crystal properties, J. Serb. Chem. Soc. 74 (2009) 1097–1104.
85. L. Mishra, V.K. Singh, Synthesis, structural and antifungal studies of Co(II), Ni(II), Cu(II) and Zn(II) complexes with new Schiff bases bearing benzimidazoles, Ind J Chem. 32 (1993) 446-457.